Journal of Climate

The climate response to multiple volcanic eruptions mediated by ocean heat uptake: damping processes and accumulation potential

--Manuscript Draft--

Manuscript Number:	JCLI-D-17-0703
Full Title:	The climate response to multiple volcanic eruptions mediated by ocean heat uptake: damping processes and accumulation potential
Article Type:	Article
Corresponding Author:	Mukund Gupta Massachusetts Institute of Technology Cambridge, MA UNITED STATES
Corresponding Author's Institution:	Massachusetts Institute of Technology
First Author:	Mukund Gupta
Order of Authors:	Mukund Gupta
	John Marshall
Abstract:	A hierarchy of models is used to explore the role of the ocean in mediating the response of the climate to a single volcanic eruption and to a series of eruptions by drawing cold temperature anomalies in to its interior, as measured by the ocean heat exchange parameter q [Wm-2K-1]. The response to a single (Pinatubo-like) volcano comprises two primary timescales, one fast (year) and one slow (decadal). Over the fast timescale, the ocean sequesters cooling anomalies induced by the eruption in to its depth, enhancing the damping rate of sea surface temperature (SST) relative to what would be expected if the atmosphere acted alone. This compromises the ability to constrain atmospheric feedback rates measured by λ [~ 1 Wm-2K-1] from study of the relaxation of SST back toward equilibrium, but yields information about the transient climate sensitivity proportional to λ + q. This study suggests that q is perhaps twice as large as λ in the immediate aftermath of an eruption. Shielded from damping to the atmosphere, the effect of the volcano persists on longer decadal timescales. This ability of the ocean to 'accumulate' the response of a succession of volcanic eruptions over time, may in part explain the prolongation of cold surface temperatures experienced during, for example, the Little Ice Age.
Suggested Reviewers:	Jonathan Gregory Professor, University of Reading j.m.gregory@reading.ac.uk Prof. Gregory would be a great reviewer for this paper, given his work on heat diffusion in the ocean and his work on simplified models of the climate.
	Timothy Merlis Assistant Professor, McGill University timothy.merlis@mcgill.ca Prof. Merlis has done work closely related to this paper in the past and hence could provide valuable feedback.

Click here to access/download
Cost Estimation and Agreement Worksheet
Journals_CEAW.pdf

The climate response to multiple volcanic eruptions mediated by ocean heat uptake: damping processes and accumulation potential

Mukund Gupta & John Marshall

Department of Earth, Atmospheric, and Planetary Sciences,

Massachusetts Institute of Technology, Cambridge, MA 02139

Email: guptam@mit.edu

Abstract

A hierarchy of models is used to explore the role of the ocean in mediating the response of the climate to a single volcanic eruption and to a series of eruptions by drawing cold temperature anomalies in to its interior, as measured by the ocean heat exchange parameter q [$Wm^{-2}K^{-1}$]. The response to a single (Pinatubo-like) volcano comprises two primary timescales, one fast (year) and one slow (decadal). Over the fast timescale, the ocean sequesters cooling anomalies induced by the eruption in to its depth, enhancing the damping rate of sea surface temperature (SST) relative to what would be expected if the atmosphere acted alone. This compromises the ability to constrain atmospheric feedback rates measured by λ [~ 1 $Wm^{-2}K^{-1}$] from study of the relaxation of SST back toward equilibrium, but yields information about the transient climate sensitivity proportional to $\lambda + q$. This study suggests that q is perhaps twice as large as λ in the immediate aftermath of an eruption. Shielded from damping to the atmosphere, the effect of the volcano persists on longer decadal timescales. This ability of the ocean to 'accumulate' the response of a succession of volcanic eruptions over time, may in part explain the prolongation of cold surface temperatures experienced during, for example, the Little Ice Age.

1. Introduction

Large volcanic eruptions are a natural, impulse-like perturbation to the climate system. The sulfur particles ejected into the stratosphere during those events are rapidly converted to sulfate aerosols that diminish the net incoming solar flux at the top of the atmosphere resulting in a cooling of the surface climate. These sulfate aerosols have an e-folding residence time of about 1-2 years in the stratosphere (Robock, 2000) but can cause surface cooling for many more years after the eruption.

The response of the climate to volcanos is of interest for at least two reasons. First, it can teach us about how robust is the climate to a perturbation and the rate at which it relaxes back to equilibrium. Second, because of its large effective heat capacity, the ocean can perhaps remember the effect of successive volcanos, enabling an accumulation larger than any single event. Some of the issues are illustrated in Fig.1, which shows the hypothetical response of the climate to a volcano in two limit cases. In the first, the atmosphere is imagined to be coupled to a slab ocean. The relaxation of the system here depends simply on the climatic feedback parameter λ [$Wm^{-2}K^{-1}$]. The larger the value of λ, the smaller the equilibrium climate sensitivity and the faster the system relaxes back to equilibrium. In the second, the slab lies atop an interior ocean that can sequester heat away from the surface at rate q [$Wm^{-2}K^{-1}$], enhancing damping of SST in the initial stages. However, on longer timescales the sequestered heat anomaly is shielded from damping to space leading to a prolongation of the signal. Thus, interaction with the interior ocean changes the response from that of a simple exponential decay on one timescale to a two-timescale process, as evidenced by the 'dog-leg' profile evident in Fig.1 which becomes more prominent as the ratio $\mu = q/\lambda$ increases.

A number of studies have explored the role of the deep ocean in the climatic response to external forcings (e.g. Hansen et al. 1985; Gregory 2000; Held et al. 2010; Geoffroy et al. 2013). Volcanic responses have been explored in simple box models (e.g. Lindzen and Giannitsis 1998) as well as in state-of-the-art global climate models (Stenchikov et al. 2009; Merlis et al. 2014). Here, we explore the role of the ocean in sequestering thermal anomalies to depth, temporarily shielding them from damping processes thereby extending the response timescale. As we shall see, this mechanism can promote accumulation of the cooling signal from successive eruptions and cause the response to span multi-decadal timescales.

This study employs a hierarchy of idealized models - ranging from a 2-box model, a 1-D diffusion model and a coupled Global Circulation Model (GCM). Section 2 displays results from idealized volcanic eruptions in a GCM; in Section 3, we interpret those results using a simple 2-box model of the ocean and investigate climate sensitivity; in Section 4, we study the climate response to the volcanic forcing of the last millennium and in Section 5 we conclude.

2. Experiments with an idealized coupled aquaplanet model

2.1 Experiment description

We use a coupled atmosphere-ocean model based on the MITgcm aquaplanet model (see Appendix A). Idealized volcanic eruptions are simulated by reducing the net surface shortwave radiative flux by a uniform amount over the globe (except in polar night regions). The forcing is applied as a 1-year square pulse in time starting January 1st. Both single and multiple pulses (separated by a specified interval) are considered. Numerical experiments are run using both a ‘slab ocean’ and a ‘full ocean’ configuration of the MITgcm.

2.2 Idealized volcanic responses

Fig. 2 shows the SST response of the MITgcm to a forcing of -4 Wm^{-2} for 1 year, which crudely emulates the radiative effect of the 1991 Mount Pinatubo eruption. A theoretical 10 × Pinatubo eruption was also simulated using a forcing of -40 Wm^{-2} for a year. Ensemble members (5 for the Pinatubo forcing and 1 the for 10 × Pinatubo forcing) were initialized from a long control integration of the model separated by 10-year intervals. Anomalies were calculated by subtracting the response of the forced run from the control run. Fig. 2 (a) shows all model responses normalized with respect to their peak cooling value. The slab ocean curves decay over a single e-folding timescale of about 4 years, whereas the full ocean curve displays an initial fast relaxation rate and a long-lasting tail (5-10% of the signal present after 20 years). The shape of these response functions are interpreted using a 2-box model of the climate in Section 3.

Fig. 2 (b) shows that in the Pinatubo-like simulations, the SST anomaly reaches a minimum value of -0.62 °C for the slab and -0.41 °C for the full ocean. This difference accounts for some of the cooling being sequestered into the deeper ocean during the first year. Soden et al. (2000) report an observed globally-averaged tropospheric temperature anomaly of -0.5°C the year after the Pinatubo eruption, broadly in accord with our calculations. The shading in Fig. 2 (b) is the envelope corresponding to the response of the various ensemble members, whereas the dotted lines are the ensemble means. In the first year, while the forcing is active, the behavior of each ensemble member shows very little variability, but the simulations diverge from each other after the forcing is turned off. The standard deviation in the SST anomaly eventually settles to 0.11°C for the full ocean and 0.06°C for the slab ocean, characteristic of the noise levels in those configurations. Fig. 2 (c) shows that for a 10 × Pinatubo forcing, the slab ocean displays a maximum cooling of -6.1°C versus only -3.7°C for the full ocean. This peak cooling scales linearly with the forcing amplitude in the slab ocean case, but is 10% smaller than linear scaling when the ocean is active. This non-linearity can be explained by the fact that the larger forcing causes the mixed layer depth to increase, which allows the cooling to penetrate deeper into the ocean. Moreover, the effect of the deeper ocean in prolonging the signal can be seen clearly by comparing the slab configuration, whose temperature anomaly reaches noise levels after 15 years and the full ocean case, whose anomaly persists at -0.2°C for 20 years at least.

Fig. 3 shows the evolution of the ocean temperature anomaly as a function of latitude and depth for the Pinatubo and 10×Pinatubo forcings (full ocean configuration). Within 2 years of the eruption, a significant amount of cooling is transported below the mixed layer. Temperature anomalies on the order of 10% of the peak surface cooling exist at 300m depth and persist for more than 10 years after the cooling pulse. A combination of processes may be acting to spread the anomaly vertically, such as turbulent diffusion, Ekman pumping, seasonal convection, mixing in the wind-driven gyres and large scale overturning circulation (e.g. Gregory 2000; Stouffer et al. 2004; Stenchikov et al. 2009). Fig. 3 shows signatures of Ekman pumping below the subtropical gyres, particularly visible for the 10×Pinatubo forcing. At the poles, the penetration of the anomaly at depth happens over a longer timescale than at the mid-latitudes. Several studies (e.g. Stenchikov et al. 2009; Otterå et al. 2010 and Mignot et al. 2011) discuss a strengthening of the meridional overturning circulation in response to volcanic eruptions, which could also contribute to the vertical exchange. For the 10×Pinatubo eruption, the globally-averaged mixed layer depth increases by about 50% (63m) in the year of the eruption and relaxes back to its base value (43m) within 3 years. This increase is principally due to reduced density stratification the tropics and could explain the slight non-linearity in the 10×Pinatubo response noted in Fig. 2.

Fig. 4 shows simulations of a series of Pinatubo-like eruptions occurring every 10 years in the slab and full ocean configurations. The full ocean displays 20% accumulation in 100 years against none for the slab, which suggests that the presence of a deeper ocean can facilitate the build-up of a cooling signal from successive eruptions. In Section 3, we discuss the conditions that can lead to signal accumulation using a 2-box model as a guide.

3. Interpretation using a 2-box model

3.1 The two timescale response

The globally-averaged SST responses of the MITgcm aquaplanet to an idealized volcanic forcing can be interpreted using simple analytical models of the climate. We find that the shapes of the temperature response functions can be recovered from both a 1-D diffusion model and a 2-box model of the ocean. For the sake of brevity and ease of interpretation we focus here on the 2-box model results. Calculations pertaining to the 1-D diffusion model are included in Appendix B. The 2-box model shown in Fig. 5 was introduced by Gregory (2000) and has subsequently been employed by Held et al. (2010), Kostov et al. (2013) and others. It consists of a mixed layer and a deeper ocean box of temperature T_1 and T_2 respectively, driven from the top by an external forcing F and damped by the climate feedback λT_1. It can be written as follows:

$$\rho c_w h_1 \frac{dT_1}{dt} = -\lambda T_1 + q(T_2 - T_1) + F(t) \qquad (1)$$

and

$$\rho c_w h_2 \frac{dT_2}{dt} = q(T_1 - T_2), \qquad (2)$$

where h_1 and h_2 are the heights of the mixed layer and deeper ocean boxes respectively. The water density and calorific heat capacity are ρ and c_w respectively. The parameter q represents vertical ocean heat exchanges. It is positive for an active deeper ocean and zero for a slab ocean. We represent an idealized volcanic eruption by imposing a delta function forcing $F(t) = V\delta(t)$

in Eq. (1), where V is the integrated amount of energy instantaneously extracted from the system. This impulse (or Green's function) response provides information on the first order climate response to a volcanic eruption and lends itself to convolution with a more realistic time series of forcing (see Section 4). The analytical solution to Eq. (1) and (2) is presented in the Supplementary Information (SI). The response of T_1 is given by:

$$T_1(t) = T_f e^{-t/\tau_f} + T_s e^{-t/\tau_s} \qquad \text{(3a)} \qquad \text{and} \qquad T_f + T_s = T_c\,, \qquad \text{(3b)}$$

where T_c, T_f, T_s, τ_f and τ_s are written out in the SI. Eq. (3) describes the relaxation of T_1 back to equilibrium after the forcing F has ceased to act. The relaxation occurs over a fast and a slow timescale with e-folding values τ_f and τ_s respectively. In the case of a delta function forcing, the peak cooling T_c occurs instantaneously at t = 0 and is given by:

$$T_c = \frac{V}{\rho c_w h_1}\,, \qquad (4)$$

where V is the integrated amount of energy extracted from the system by the forcing:

$$V = \int_0^\infty F(t)dt\,. \qquad (5)$$

Eq. (4) suggests that the peak cooling T_c does not depend on the climatic feedback λ and oceanic damping q, but this is only valid for an idealized instantaneous forcing, as will be seen in Section 3.3.

We also introduce the parameters μ and r:

$$\mu = \frac{q}{\lambda} \qquad \text{(6a)} \qquad \text{and} \qquad r = \frac{h_1}{h_2}\,. \qquad \text{(6b)}$$

The parameter μ represents the ratio of the ocean damping strength versus climatic damping, and r is the ratio of heat capacities between the two boxes. In the SI, we show that in the limit of small r, the parameters T_f, T_s, τ_f and τ_s are given by:

$$\tau_f \approx \frac{\rho c_w h_1}{\lambda(1+\mu)}, \qquad (7a) \qquad\qquad \tau_s \approx \rho c_w h_1 \frac{(1+\mu)}{qr}, \qquad (7b)$$

$$T_f \approx \frac{(1+\mu)^2}{(1+\mu)^2 + r\mu^2} T_c \qquad (8a) \qquad \text{and} \qquad T_s \approx \frac{r\mu^2}{(1+\mu)^2 + r\mu^2} T_c\,. \qquad (8b)$$

When $\mu \ll 1$, the transfer of heat to the deeper ocean is limited and the atmosphere is the only significant medium responsible for the damping of the anomaly. We refer to the limiting case of no ocean mixing (μ and q = 0) as the 1-box model, where the solution reduces to a single exponential decay, set by damping to the atmosphere:

$$T_1(t) = T_c\, e^{-t/\tau_m}\,, \qquad (9a) \qquad\qquad \text{with } \tau_m = \frac{\rho c_w h_1}{\lambda}. \qquad (9b)$$

When $\mu \gg 1$, i.e. when ocean heat transport is large relative to climatic damping, we obtain:

$$\tau_f \approx \frac{\rho c_w h_1}{q}, \qquad (10a) \qquad\qquad \tau_s \approx \frac{\rho c_w h_2}{\lambda}, \qquad (10b)$$

$$T_f \approx \frac{T_c}{1+r} \qquad (11a) \qquad \text{and} \qquad T_s \approx \frac{r}{1+r} T_c. \qquad (11b)$$

In this limit it is interesting (and curious) to note that the fast timescale is controlled by oceanic damping q, whereas the slow timescale is controlled by the climatic feedback λ. The two timescales lead to the 'dog-leg' profile evident in Fig. 1 which becomes more prominent as the ratio μ increases. Physically, we can understand this as a rapid initial stage during which the temperature anomaly is sequestered in the deeper ocean, followed by a slower stage over which the anomaly is damped by climatic feedbacks. In this limit, the coefficients T_f and T_s only depend on T_c and r.

3.2 Parameter fitting

Fig. 6 (a) shows the 1-box and 2-box model fits to the MITgcm slab and full ocean responses respectively. The value of h_1 is set to 43m, the globally and annually averaged mixed layer depth diagnosed from a long control simulation. To estimate λ, we use the equilibrium response of the slab ocean configuration to a constant and spatially uniform forcing F_s. Setting $F(t) = F_s$ in Eq. (1) produces a response that asymptotes to the equilibrium climate sensitivity (ECS):

$$ECS = \frac{F_s}{\lambda}. \tag{12}$$

Setting $F_s = -4$ Wm^{-2} produces an asymptotic response of -2.67 °C, giving $\lambda = 1.5$ $Wm^{-2}K^{-1}$. We then use least-square minimization with respect to the full ocean Pinatubo response in Fig. 2 (b). to obtain $q = 3.5$ $Wm^{-2}K^{-1}$ and $h_2 = 150$m with a fitting accuracy of $r^2 = 0.87$. The fit to the slab ocean configuration is obtained simply by setting $q = 0$ and gives a fitting accuracy of $r^2 = 0.97$. The e-folding relaxation time of the slab ocean curve is $\tau_m = 4$ years, whereas the fast and slow timescales corresponding to the full ocean simulations are $\tau_f = 1$ year and $\tau_s = 22$ years respectively. Parameter values are summarized in Table 1.

Fig. 6 (b) shows the time evolution of T_1 and T_2, along with the response of the MITgcm globally-averaged SST and temperature at 120m depth. Immediately after the eruption, the large temperature difference between the mixed layer and the deeper ocean leads to large vertical heat exchange, with surface cooling being sequestered into the thermocline. In this first phase of relaxation, while T_2 decreases, ocean heat exchanges assist climatic feedbacks in damping the response of the mixed layer. The fast (1-year) timescale τ_f given by Eq. (5a) provides an estimate of the initial decay timescale of the response, which is thus set by $\lambda + q$. Since $\mu = 2.3$, we conclude that ocean damping is very important in the first few relaxation years. Subsequently, when T_1 and T_2 are nearly equal, the system behaves like a single box with a combined thickness $h_1 + h_2$ that relaxes over a longer (20-year) timescale. In effect, the heat sequestration by ocean damping temporarily shields the cooling from the damping mechanisms at the surface and thus promote the lingering of the cooling signal. These results are consistent with the work of Wigley et al. (2005), who reported a sharp (2-3 years) decay timescale after the eruption followed by a long 'tail' in the signal.

3.3 Climate sensitivity and the relative importance of atmospheric and oceanic damping

A number of studies (e.g. Lindzen & Giannitsis, 1998; Wigley et al. 2005; Yokohata et al. 2005; Hegerl et al. 2006; Bender et al. 2010; Merlis et al. 2014) have attempted to relate the surface temperature response from volcanic eruptions to some measure of the climate sensitivity. Lindzen and Giannitsis (1998) simulated volcanic eruptions using a 1-D box diffusion model with a range of ECS values (as defined in Eq. (11)) to argue that high ECS values are not realistic, because they produces much longer prolongation than seen in observations. However, Wigley et al. (2005) have argued that the amount of signal prolongation simulated by Lindzen and Giannitsis (1998) is likely an overestimate and find that an ECS as high as 4.5°C per doubling of CO_2 ($F_s = 3.7$ Wm^{-2}) cannot be discarded. Yokohata et al. (2005) rule out very high sensitivities (6.3°C) but find in their model that an ECS of 4.0°C produces results consistent with observations.

We start our investigation of the climate sensitivity by simulating idealized Pinatubo eruptions in the 2-box model for increasing λ values (decreasing ECS, see Fig. 7). All other parameters are kept constant and set to those in Table 1. As expected, the response magnitude reduces at all times for larger λ. For the same values of mixed layer depth and ECS, we obtain significantly shorter prolongation timescales than those recorded by Lindzen and Giannitsis (1998) both in the 2-box model and in the 1-D diffusion model (Appendix B). Instead, our results are more consistent with the typical decay timescales found by Santer et al. (2001) and Wigley et al. (2005).

Three different methods have been use to quantify climate sensitivity from the response to a volcano, by linking: (i) the peak cooling to the ECS (ii) the integrated response to the ECS and (iii) the integrated response to the transient climate sensitivity (TCS). In what follows, we review these methods and evaluate them based on the results we obtained from the curve fitting procedure detailed in Section 3.2.

(i) Peak cooling and ECS

Fig. 7 shows that the peak cooling after volcanic eruptions tends to decrease with increasing values of λ. Past studies (e.g. Wigley et al. 2005; Bender et al. 2010) have attempted to link this peak cooling to λ (or the ECS), but did not find a strong correlation between the two quantities. Generally, the effect of noise is invoked to explain this lack of correlation. The 2-box model can be used to explore this idea further. We invoke Eq. (1) to obtain an approximate expression for the peak cooling T_c after a pulse forcing that lasts a small but finite time Δt (see SI):

$$T_c \approx \frac{V}{\rho c_w h_1 + \frac{\lambda \Delta t (1+\mu)}{2}}. \tag{13}$$

It is easy to show that Eq. (13) simplifies to Eq. (4) when Δt tends to zero. When the forcing time is finite however, the peak cooling T_c depends on both the climate feedback λ and the ocean damping q (through the parameter μ). In the limit of small μ, the ocean does not play a significant role and in theory the value of λ could be inferred from knowledge of V, T_c, Δt and h_1. However if $\mu \geq 1$, oceanic damping becomes as important as λ in reducing T_c and hence any correlation between these two quantities can be confounded by the influence of ocean heat sequestration. Moreover, Fig. 7 shows that the influence of λ on the peak cooling is relatively small (especially for small Δt) and can easily be obscured by noise, as argued by Wigley et al. (2005) and Bender et al. (2010).

(ii) Integrated response and ECS

To mitigate against the effect of noise, previous studies (e.g. Yokohata et al. 2005; Bender et al. 2010; Wigley et al. 2005) have proposed to link the ECS to the time-integrated volcanic response, rather than just the peak cooling value. This approach can also be interpreted in terms of the 2-box model, by integrating Eq. (1) in time from t = 0 to ∞, giving:

$$\lambda \int_0^\infty \mathrm{T}_1(\mathrm{t})\mathrm{dt} = V. \qquad (14)$$

Eq. (14) is a statement of conservation of energy: the energy extracted from the system by the volcanic eruption (RHS) must be balanced by the total energy recovered through climatic feedbacks (LHS) over the entire duration of the process. We note here parenthetically that since the time integrated response does not depend on ocean damping, the presence of an active deeper ocean underneath the mixed layer does not change the value of the integrated temperature response. A larger value of q tends to shift the weight of the response towards longer timescales, without affecting the ‘area under the curve’ (see Fig. 1).

The absence of the parameter q in Eq. (14) also means that the time integrated response can in theory be used to infer λ (or the ECS), without the conflating influence of ocean damping. A common problem however is that in complex GCMs and observations, the response typically becomes indistinguishable from noise 5-10 years after Pinatubo-like eruptions. If μ is small, the timescale of the response is dominated by the mixed layer and in that case, an integration time of 5-10 years may be enough to obtain a reliable estimate of λ. However if μ is large, a significant part of the cooling energy is still stored in the ocean during that period, and using Eq. (14) for such a short integration time is likely to give an overestimate of λ. Moreover, Fig. 7 shows that the response curves (corresponding to different λ values) are tightly packed in the initial fast decay stage (0-3 years) but later become more distinct from each other (3-20 years). This overall behavior is reflective of the conclusion we drew from Eq. (10), that in the limit of large μ, the fast timescale is controlled by q, whereas the slower timescale is set by λ. This limits the usefulness of Eq. (14) for estimating the ECS.

(iii) Integrated response and TCS

Since the volcanic SST signal rapidly fades to noise for typical modern-era volcanic eruptions, Merlis et al. (2014) suggested that the SST response could provide a more reliable constraint on the transient climate sensitivity (TCS) instead of the long term ECS. The TCS is a measure of the response of the system while the deep ocean temperature has not been significantly affected by the forcing and has been suggested as a more relevant parameter to characterize the evolution of the climate under anthropogenic CO_2 forcing (e.g. Held et al. 2010). The TCS can be derived by enforcing $T_2 \ll T_1$ in Eq. (1):

$$\rho c_w h_1 \frac{dT_1}{dt} \approx -(\lambda + q)T_1 + F(t)\,. \qquad (15)$$

Solving Eq. (15) at equilibrium with $F(t) = F_s$ as in Eq. (11) then yields the TCS:

$$TCS = \frac{F_s}{\lambda + q}\,. \qquad (16)$$

The TCS is inversely proportional to the sum λ + q, as is the approximate fast timescale τ_f given in Eq. (7a). The TCS can therefore be interpreted as the characteristic response over that fast timescale. To estimate the TCS, Merlis et al. (2014) propose to integrate Eq. (15) up to a time t_I short enough that $T_2 \ll T_1$, but long enough that the LHS of Eq. (15) becomes negligible. It is also assumed that the forcing has ceased to act before time t_I. The energy balance then becomes:

$$(\lambda + q) \int_0^{t_I} T_1(t)dt \approx V. \tag{17}$$

Eq. (17) states that the energy extracted by the forcing is approximately balanced by the energy dissipated by both atmospheric and oceanic damping up to time t_I and should be contrasted with Eq. (14). Merlis et al. (2014) use a value of t_I = 15 years and find values of λ + q that are on the order of 2 $Wm^{-2}K^{-1}$. They also estimate the value of λ separately, by consideration of the top of atmosphere radiation balance and find q and λ values both on the order of 1 $Wm^{-2}K^{-1}$. Using t_I = 15 years, we apply this method to the 2-box model fit of the MITgcm full ocean simulation shown in Fig. 6 (a) to obtain λ + q = 2.9 $Wm^{-2}K^{-1}$, giving q = 1.4 $Wm^{-2}K^{-1}$. This is a large underestimate of the value of q = 3.5 $Wm^{-2}K^{-1}$ that was found from curve fitting and subsequently used as an input to the 2-box model.

In this study, we argue based on Fig. 6 (b), that an integration time of t_I = 1-3 years may be more appropriate to satisfy the condition $T_2 \ll T_1$. Beyond that time, the deeper layer temperature anomaly (at around 120m depth) is of the same order of magnitude as the mixed layer temperature anomaly. However, we note that such a short time after the eruption is not long enough to neglect the LHS of Eq. (15), as was done to obtain Eq. (17). Hence, we integrate Eq. (15) again, but this time taking account of the transient term on the LHS to give:

$$(\lambda + q)\int_0^{t_I} T_1(t)dt \approx V - \rho c_w h_1 T_1(t_I). \quad (18)$$

Eq. (18) can be used to estimate λ + q more accurately than with Eq. (17), but requires knowledge of h_1 in addition to V and $T_1(t)$. Using Eq. (18) with t_I = 3 years, we find λ + q = 4.4 $Wm^{-2}K^{-1}$ and q = 2.9 $Wm^{-2}K^{-1}$. This is still an underestimate of the value of the curve fit value (q = 3.5 $Wm^{-2}K^{-1}$, but better than the one obtained using Eq. (17) and t_I = 15 years. Further tests with a range of q values in the 2-box model find that shorter integration times give more accurate results, but that this method tends to underestimate q values. The method is also less accurate for large q values because they lead to a rapid increase in the magnitude of T_2, causing the approximation $T_2 \ll T_1$ to break down after only a short time. Nevertheless, Eq. (18) can provide a way forward to estimate the TCS from knowledge of the SST response, h_1 and V.

3.4 Accumulation potential

In Fig. 8, we use the 2-box model to assess the accumulation potential of the SST response from successive volcanic eruptions. We develop a metric for accumulation by considering a series of uniform eruptions spaced at a regular interval τ. As was seen in the aquaplanet simulations in Fig. 4, the peak magnitude of the response may increase over time if the response decay timescale is small relative to the interval between each eruption. We apply the mathematical formula for the sum of a geometrical series to calculate the peak temperature response after each eruption to obtain T_{en} the envelope of the signal (see SI):

$$T_{en}(t) = T_f \frac{1 - e^{-(t+\tau)/\tau_f}}{1 - e^{-\tau/\tau_f}} + T_s \frac{1 - e^{-(t+\tau)/\tau_s}}{1 - e^{-\tau/\tau_s}}. \quad (19)$$

In the theoretical limit that the repeated eruptions occur for all time (t → ∞), the envelope asymptotes to a finite value T_∞ given by (see SI):

$$T_\infty = \frac{T_f}{1 - e^{-\tau/\tau_f}} + \frac{T_s}{1 - e^{-\tau/\tau_s}}\,. \qquad (20)$$

This limit is reached when the rate at which cooling is supplied by the eruptions equals the rate at which it is extracted out by the climate feedbacks. Eq. (20) thus provides a theoretical maximum to the temperature accumulation resulting from successive uniform eruptions. The analytical expression for T_∞ explicitly reveals how the potential for accumulation increases when the ratios τ/t_f and τ/t_s decrease. The limit T_∞ is analogous to the equilibrium climate response under a step forcing and in fact tends to the ECS as the interval between the eruptions approaches zero. The fast and slow components of T_∞ are of the same order of magnitude so they both matter to the response, even in the limit when μ is large. On the other hand, when μ is small, the response is dominated by the mixed layer timescale, which then controls the accumulation potential.

In Fig. 8, we explore the sensitivity of the temperature envelope T_{en} to the following parameters: λ, q, h_1 and τ. The build-up amount is expressed relative to the peak cooling after the first eruption in the series, which varies with h_1, λ and q (see Eq. (13)). The blue points in each panel describe the accumulation curve obtained with the parameters from the 2-box fit to the MITgcm response (see Table 1). Fig. 8 (a) and (b) show that a smaller climate sensitivity λ and a larger mixed layer depth h_1 elicit a larger accumulation potential T_{en}. Both these parameters directly affect the relaxation of the mixed layer temperature and hence are of primary importance in setting the amount of response build-up. Fig. 8 (c) shows the effect of the ocean mixing q in increasing the accumulation potential T_{en}. A comparison with the aquaplanet results from Fig. 4 shows that the 2-box model (q = 3.5 $Wm^{-2}K^{-1}$) quantitatively captures the 20% accumulation seen in the full ocean configuration. Conversely, the 1-box model (q = 0) displays the same absence of accumulation as was observed in the slab configuration. Fig. 8 (d) shows the increase in response build-up as the interval between eruptions τ is narrowed. It reveals that eruptions spaced by more than 20 years have a very low accumulation potential. Overall, the results of this analysis show that for the range of parameters considered, a regular series of uniform eruptions can yield a maximum accumulation of approximately 10-50%. Moreover, ocean heat sequestration favors accumulation, as demonstrated with the behavior of T_{en} with increasing mixing parameter q and mixed layer depth h_1.

4. Response to the last millennium volcanic forcing

The role of the ocean in time prolonging the climate signal can be seen at work in the context of the volcanic forcing over the last millennium. A growing number of studies (e.g. Crowley, 2000; Hegerl et. al, 2003; Atwood et al. 2016) have highlighted the importance of volcanic eruptions in instigating the coldest period of the Holocene, commonly referred to as the Little Ice Age (LIA, ~1250-1850 CE). They point to volcanic cooling as a major contributor to the LIA, beyond the effects of reduced insolation, changes in greenhouse gases, and land use evolution. Some authors (e.g. Free et al. 1999; Crowley et al. 2008; Stenchikov et al. 2009) have already suggested that the ocean's long response timescales could help explain how eruptions that typically last only 1-2 years could engender cooling over multiple decades. Here, we make use of the MITgcm and the 2-box model to investigate the magnitude of signal prolongation due to ocean damping and the relative importance of small versus large eruptions.

Fig. 9 (adapted from Sigl et al. 2015) shows a reconstruction of Europe and Arctic temperatures along with global volcanic activity over the past 2500 years. The two panels show that 20 of the 40 coldest years in the series occurred during the Little Ice Age (LIA) and that those cold years coincided with the largest eruptions of that period. The LIA was characterized by the occurrence of cold spells during the mid 15th, 17th and early 19th century. The spatial extent of the cooling is not yet known as most proxy records originate from land in the Northern hemisphere. Nevertheless, Neukom et al. (2014) provide some indications that sustained periods of cooling occurred in the Southern hemisphere, particularly in the 17th century. In this study, we focus on large tropical volcanic eruptions, because the stratospheric transport of particles towards the poles results in a considerable global climatic impact (Robock, 2000). Moreover, the volcanic forcing reconstruction in Fig. 9 (b) indicates that tropical eruptions were larger than hemispheric ones in the past 2500 years. We choose the LIA as an example of a modern period with intense tropical volcanic activity to investigate whether the presence of a deep ocean can extend the response from individual eruptions and create periods of sustained decadal cooling, as observed in the historical record.

Fig. 10 (a) shows an estimate of the volcanic forcing of the last millennium (A. LeGrande, NASA GISS, personal communication). It reveals the large volcanic eruptions of the 13th, 15th, 17th and 19th centuries as well as the smaller ($< 4 Wm^{-2}K^{-1}$) eruptions that occurred more regularly throughout the timeseries. In Fig. 10 (b) and (c), we plot the MITgcm response to this historical volcanic forcing, in the form of the globally-averaged SST anomalies for the slab and full ocean configurations. These panels show that SSTs in the full ocean scenario tend to be colder than in the slab for the decades following clusters of large volcanic eruptions (13th, 15th, 17th and 19th centuries). Note that since the model does not contain ice, it does not capture the positive sea-ice feedback proposed by Miller et al. (2012) that link volcanism and the LIA. The differences in responses between the slab and full ocean configurations can be attributed to the sequestration of cold anomalies by the deeper ocean.

Fig. 10 (c) shows that the strong volcanic activity of the 13th century, which has previously been related to the onset of the LIA (e.g. Miller et al. 2012; Cole-Dai et al. 2013) has an effect that spans multiple decades. At the end of this sequence of eruptions, the temperature anomaly in the full ocean configuration remains mostly colder than the slab until the middle of the 15^{th} century. Similarly, after the large 1450's eruptions (Cole-Dai et al. 2013) the full ocean configuration displays a temperature anomaly of around -0.2°C that lasts for around 100 years, in contrast to the slab, whose response decays to noise after about 20 years. There is also some signal prolongation after the 17^{th} century eruptions, which persists for around 20 years at the beginning of the 1800's. Finally, as reported by Crowley et al. (2008), the close packing of four eruptions between 1809 and 1835 (including the Tambora eruption in 1815) leads to an accumulated climate response in the 19^{th} century, because of the long timescales imparted by the global oceans.

Fig. 10 (d) shows the historical forcing responses of the box model obtained using the parameters in Table 1. Comparing Fig. 10 (b) and (d) shows that the box model reproduces the temperature anomalies of the MITgcm slab and full ocean configurations relatively well, indicating that the response remains mostly linear even on centennial timescales. However, as discussed in Section 2.2, very large eruptions in the MITgcm full ocean configuration induce some non-linearity due to increased mixed layer depths and a deeper sequestration of the cooling, particularly in the tropics. This causes a 10% decrease in the peak response relative to the linear case (approximately) but also a longer tail. The 2-box model does not capture this extra amount of signal prolongation from large forcings, since it is calibrated to a Pinatubo-size eruption. Nevertheless, the 2-box model temperature is colder than the 1-box model temperature during 70% of the simulation, clearly highlighting the importance of the deeper ocean in extending the response. Fig. 10 (c) also shows the sensitivity of the box model to various values of the climate feedback λ, ranging from 0.8 to 2.5 $Wm^{-2} K^{-1}$. Small values of λ lead to longer prolongation as anticipated in Section 3, but without notable qualitative changes in the response.

In Fig. 10 (e), we use the 2-box model to estimate the contribution of the response from small eruptions (less than or equal to -4 Wm^{-2}) versus large eruptions (greater than -4 Wm^{-2}). We find that small eruptions are frequent enough that their responses accumulate and cool the climate almost continuously throughout the entire timeseries by about 0.05°C. Large eruptions occur more rarely but can still lead to accumulation, e.g. 13th and 19th centuries. These results show that both small and large eruptions played an important part in the cooling of the climate during the last millennium. Moreover, the large volcanic eruptions from 1250 to 1850, coupled with the heat sequestration from the deeper ocean, could have been a significant driver of the extended periods of cooling observed during the LIA.

5. Discussion and conclusions

We explore the role of the ocean in modulating the globally-averaged SST response of the climate to volcanic cooling, using a hierarchy of idealized models. We find that the presence of the deeper ocean beneath the mixed layer introduces a 'dog-leg' response characterized by two timescales. This effect strengthens with the parameter μ, which characterizes the ratio of ocean damping q and climatic feedback λ. In our study, curve-fitting the MITgcm response to a 2-box model gives $q = 3.5\ Wm^{-2}K^{-1}$, $\lambda = 1.5\ Wm^{-2}K^{-1}$ and $\mu = 2.3$. This large value of μ leads to a pronounced 'dog-leg' in the response, with fast and slow timescales of 1 and 20 years respectively. This result can be contrasted to the work of Merlis et al. (2014) who report $\mu \approx 1$ and Douglass et al. (2006) who find that heat exchange anomalies between the mixed layer and the thermocline were small after the 1991 Pinatubo eruption.

In the limit of large μ, we show perhaps surprisingly, that the fast timescale is dominated by ocean damping, whereas the slow one is controlled by atmospheric feedbacks. Thus in the first few years following the eruption, heat exchange with the deeper ocean dominates over the climatic feedbacks in relaxing the SST response, sequestering the (negative) heat in the ocean interior and reducing the magnitude of the peak anomaly. Subsequently, the cooling stored in the deeper ocean is delivered back to the surface over decadal periods, extending the response beyond the timescale implied by a slab ocean configuration.

We went on to review several methods for constraining climate sensitivity using the global-mean SST response of the climate to a volcanic eruption: (i) peak cooling, (ii) integrated response to estimate the ECS and (iii) integrated response to estimate the TCS. We argue that typical signal noise in the response is a strong limiting factor. For methods (i) and (ii), we find that results can additionally be confounded by the effects of ocean heat sequestration if q is large. Moreover, we find that using method (iii) with short integration times could in theory give reasonable estimates for q, but only if q is relatively small. The q parameter may also vary depending on the strength and duration of the forcing, due to how deep the response penetrates into the ocean.

For a forcing of the magnitude and duration of the Pinatubo eruption, we find that about 300m of the ocean beneath the mixed layer plays a role in the response. This is much smaller for example than in Kostov et al. (2013) and Geoffroy et al. (2013) who consider anthropogenic CO_2 forcing and find an h_2 parameter close to 1000m. These deeper oceanic layers associated with the ocean's meridional overturning circulation are unlikely to be excited by a Pinatubo-like eruption. Hence, the q parameter obtained from studies of volcanic cooling may differ from the ones relevant to anthropogenic CO_2 forcing. Indeed, the results from Romanou et al. (2017) suggest a strong dependence of q with time because different components of the ocean circulation become activated as time progresses. Similarly, λ also changes in time in a manner that depends on regional feedbacks mediated by ocean heat transport (e.g. Armour et al. 2012). Clearly a study of the response of the climate to a single volcanic eruption can only address the short (year to decadal) rather than the long (centennial) timescales.

Moreover, when $\mu \geq 1$, the resulting 'dog-leg' in the SST anomaly implies a longer prolongation of the response, which favors accumulation from successive eruptions. When forced by Pinatubo-like eruptions every 10 years, the full ocean simulations show 20% accumulation versus none for the slab. The accumulation occurs rather linearly in the GCM and can thus be represented by the 2-box model. We find that there is a limit to the theoretical maximum amount of accumulation that can occur for a series of regularly-spaced uniform eruptions, which decreases with the climatic feedback λ and increases with the mixed layer depth h_1. For typical parameter values, this maximum accumulation potential is around 10-50% of the initial peak cooling. We also note that the accumulation rate and propensity decrease sharply when the interval between eruptions becomes larger than the slow decay timescale (20 years).

Finally, we demonstrate how signal prolongation and accumulation due to the presence of the deeper ocean reservoir could help explain the extended periods of cooling observed during the Little Ice Age (LIA, ~1250-1850 CE). After the large clusters of eruptions of the 13^{th}, 15^{th}, 17^{th} and 19^{th} century, the deeper ocean prolongs the surface cooling over multiple decades. After the large 1450's eruptions in particular, we find a globally-averaged SST anomaly of -0.2°C that lasts for 100 with an active ocean versus 20 years with a slab ocean. When calibrated for a Pinatubo-like forcing, the 2-box model provides a reasonable representation of the MITgcm historical response, but tends to underestimate the signal prolongation after much larger eruptions ($\gg 4$ Wm^{-2}) because it does not capture the deepest sequestration of cold anomalies.

The box model reveals that the frequent small scale eruptions tended to cool the climate almost continuously by about 0.05°C throughout the last millennium. Larger eruptions were rarer, but aided by ocean heat sequestration, could have played an important part in extended periods of cooling during the LIA. These results are in line with the conclusions from Crowley et al. (2008), Miller et al. (2012), Cole-Dai et al. (2013), Atwood et al. (2016) and others. We thereby conclude that the mechanisms responsible for storing volcanic cooling in the subsurface ocean are relevant for questions pertaining to climate variability over decadal to millennial timescales.

Acknowledgements

MG acknowledges support from the John H. Carlson fellowship and JM from the NSF FESD Ozone project. We would like to thank Allegra Legrande from NASA GISS for her support in this work and for the data on volcanic forcing during the last millennium. We are also most grateful for informative discussions with Susan Solomon, Jean-Michel Campin, Brian Green and Paul O’Gorman.

Appendix A: MITgcm coupled model

This study employs the Massachusetts Institute of Technology Global Circulation Model (MITgcm; Marshall et al. 1997a,b). The model simulates the physics of an ocean-covered planet coupled to an atmosphere, with no land, sea-ice or clouds. Geometrical constraints are imposed on the ocean circulation through the effect of two narrow barriers extending from the North Pole to 35°S and set 90° apart. These barriers extend from the seafloor (assumed flat) to the surface and separate the ocean into a large and a small basin that are connected to the south. Despite the simplicity of the geometry, this ‘double-drake’ configuration of the model displays remarkably similar characteristics to the present climate, including realistic energy transports by the oceans and atmosphere, and a deep meridional overturning circulation that is dominated by the small basin (Ferreira et al. 2009).

The atmosphere and ocean fluids both use the same C32 cubed-sphere grid (32×32 points per face), yielding a nominal horizontal resolution of 2.8° (Adcroft et al. 2004; Adcroft and Campin 2004). The ocean is uniformly 3.4 km deep and has 15 vertical levels with a resolution increasing from 30 m at the surface to 400 m at depth. Effects of mesoscale eddies are parameterized as an advective process (Gent & McWilliams, 1989) and isopycnal diffusion (Redi, 1982). Convective adjustment is implemented as an enhanced vertical mixing of temperature and salinity and is used to represent ocean convection (Klinger and Marshall 1995). The background vertical diffusion is uniform and set to 3·10-5 m2s-1.

The atmospheric component of the model has 26 pressure levels and employs a gray radiation scheme with parameterized convection and precipitation as in Frierson et al. (2006).The longwave optical thickness is modified by the distribution of water vapor, following Byrne & O'Gorman (2012). In this simplified radiation scheme, the shortwave flux does not interact with the atmosphere and hence the planetary albedo is the same as the surface albedo. A seasonal cycle of insolation at the top of the atmosphere is specified for a solar constant of 1360 Wm-2. The meridional albedo contrast is represented by a pole-to-equator albedo gradient varying linearly from 0.6 to 0.2, in line with the observations presented in Donohoe and Battisti (2011).

We also make use of a ‘slab ocean’ configuration of the MITgcm that has a single layer in the vertical, whose thickness is fixed in time but varies spatially according to the annual-mean mixed layer depth diagnosed from a long control simulation. Surface heat fluxes are imposed as a stationary boundary condition to the slab ocean model. These heat fluxes are also diagnosed from the control simulation and represent ocean energy transport convergence into a given grid box.

Appendix B: The 1-D diffusion model

1-D diffusion models such as the one presented in Fig. A1 have been employed in previous studies to represent processes occurring in the global ocean (e.g. Lindzen & Giannitsis, 1998). The model considered in this paper consists of a mixed layer of uniform temperature T1 and depth h1 above a diffusive layer of finite depth H with temperature T(z). The mixed layer is forced from the top by a forcing F and climate feedbacks λT1. In the diffusive layer, the thermal diffusivity is κ. For consistency with the rest of the analysis, the mixed layer depth and climate sensitivity parameter are fixed to the following values: h1 = 43m and λ = 1.5 Wm-2K-1. The depth H is chosen to be 1000m, far enough into the depth of the ocean for the temperature anomalies after a volcanic eruption to be negligible. The model satisfies:

$$\rho c_w h_1 \frac{dT_1(t)}{dt} = F(t) - \lambda T_1(t) - \rho c_w \kappa \frac{\partial T(z=-h_1,t)}{\partial z} \qquad \text{(A9)}$$

and $$\frac{\partial T(z,t)}{\partial t} = \frac{\partial}{\partial z}\left(\kappa \frac{\partial T(z,t)}{\partial z}\right) \tag{A10}$$

With boundary conditions: $$T(z=0,t) = T_1(t) \tag{A11}$$

and $$\frac{\partial T(z=-H,t)}{\partial z} = 0 \tag{A12}$$

This set of equations are solved numerically. Fig. A2 shows a good fit between the simple model and the full ocean MITgcm configuration for $\kappa = 10^{-4}$ m^2s^{-1}. Moreover, the 1-D model solution tends to the slab solution as the diffusivity becomes very small ($\kappa = 10^{-7}$ m^2s^{-1}). In the presence of an active deeper ocean, the diffusion model reproduces the reduced peak cooling and the prolonged response that was observed in the 2-box model and in the MITgcm full ocean configuration.

Fig. A3 shows that after 3 years, the diffusion model and the MITgcm have a similar temperature evolution with depth. The magnitude of the temperature anomaly decreases with time over the top layers of the ocean and increases in the layers underneath through the combined action of the climatic feedbacks at the surface and the ocean exchanges drawing cold temperatures into the ocean depth.

References

Adcroft, A., Campin, J.-M., Hill, C., & Marshall, J. (2004). Implementation of an Atmosphere–Ocean General Circulation Model on the Expanded Spherical Cube. Monthly Weather Review, 132(1996), 2845–2863. doi:10.1175/MWR2823.1.

Adcroft, A., & Campin, J. M. (2004). Rescaled height coordinates for accurate representation of free-surface flows in ocean circulation models. Ocean Modelling, 7(3–4), 269–284. doi:10.1016/j.ocemod.2003.09.003

Armour, K. C., Bitz, C. M., & Roe, G. H. (2013). Time-varying climate sensitivity from regional feedbacks. Journal of Climate, 26(13), 4518-4534. doi:10.1175/JCLI-D-12-00544.1

Atwood, A. R., Wu, E., Frierson, D. M. W., Battisti, D. S., & Sachs, J. P. (2016). Quantifying climate forcings and feedbacks over the last millennium in the CMIP5/PMIP3 models. Journal of Climate.

Bender, F. A. M., Ekman, A. M., & Rodhe, H. (2010). Response to the eruption of Mount Pinatubo in relation to climate sensitivity in the CMIP3 models. Climate dynamics, 35(5), 875-886.

Byrne, M. P., & Gorman, P. A. (2012). Land – Ocean Warming Contrast over a Wide Range of Climates : Convective Quasi-Equilibrium Theory and Idealized Simulations. Journal of Climate, 26, 4000–4016. http://doi.org/10.1175/JCLI-D-12-00262.1

Cole-Dai, J., Ferris, D. G., Lanciki, A. L., Savarino, J., Thiemens, M. H., & McConnell, J. R. (2013). Two likely stratospheric volcanic eruptions in the 1450s CE found in a bipolar, subannually dated 800 year ice core record. Journal of Geophysical Research: Atmospheres, 118(14), 7459-7466.

Crowley, T. J. (2000). Causes of Climate Change Over the Past 1000 Years. Science, 270. http://doi.org/10.1126/science.289.5477.270

Crowley, T. J., Zielinski, G., Vinther, B., Udisti, R., Kreutz, K., Cole-Dai, J., & Castellano, E. (2008). Volcanism and the little ice age. PAGES news, 16(2), 22-23.

Donohoe, A., & Battisti, D. (2011). Atmospheric and Surface Contributions to Planetary Albedo. Journal of Climate, 24, 4402–4418. http://doi.org/10.1175/2011JCLI3946.1

Douglass, D. H., Knox, R. S., Pearson, B. D., & Clark, A. (2006). Thermocline flux exchange during the Pinatubo event. Geophysical Research Letters, 33(19).

Ferreira, D., Marshall, J., & Campin, J.-M. (2009). Localization of Deep Water Formation : Role of Atmospheric Moisture Transport and Geometrical Constraints on Ocean Circulation. Journal of Climate, 23, 1456–1476. http://doi.org/10.1175/2009JCLI3197.1

Free, M., & Robock, A. (1999). Global warming in the context of the Little Ice Age. Journal of Geophysical Research: Atmospheres, 104(D16), 19057-19070.

Frierson, D. M. W., Held, I. M., & Zurita-Gotor, P. (2006). A Gray-Radiation Aquaplanet Moist GCM. Part I : Static Stability and Eddy Scale. Journal of the Atmospheric Sciences, 63, 2548–2566.

Gent, P., & McWilliams, J. (1989). Isopycnal mixing in ocean circulation models. Journal of Physical Oceanography, 20.

Geoffroy, O., Saint-Martin, D., Bellon, G., Voldoire, A., Olivié, D. J. L., & Tytéca, S. (2013). Transient climate response in a two-layer energy-balance model. Part II: Representation of the efficacy of deep-ocean heat uptake and validation for CMIP5 AOGCMs. Journal of Climate, 26, 1859–1876. http://doi.org/10.1175/JCLI-D-12-00196.1

Green, B., & Marshall, J. (2017). Coupling of Trade Winds with Ocean Circulation Damps ITCZ Shifts. Journal of Climate, 30(12), 4395-4411.

Gregory, J. M. (2000). Vertical heat transports in the ocean and their effect on time-dependent climate change. Climate Dynamics, 16, 501–515. http://doi.org/10.1007/s003820000059

Hansen, J., Russell, G., Lacis, A., Fung, I., Rind, D., & Stone, P. (1985). Climate response times: dependence on climate sensitivity and ocean mixing. Science, 229, 857-860.

Hegerl, G. C., Crowley, T. J., Baum, S. K., Kim, K., & Hyde, W. T. (2003). Detection of volcanic , solar and greenhouse gas signals in paleo-reconstructions of Northern Hemispheric temperature. Geophysical Research Letters, 30, 94–97. http://doi.org/10.1029/2002GL016635

Held, I. M., Winton, M., Takahashi, K., Delworth, T., Zeng, F., & Vallis, G. K. (2010). Probing the Fast and Slow Components of Global Warming by Returning Abruptly to Preindustrial Forcing. Journal of Climate, 23(9), 2418–2427. http://doi.org/10.1175/2009JCLI3466.1

Klinger, B. A., & Marshall, J. (1995). Regimes and scaling laws for rotating deep convection in the ocean. Dynamics of Atmospheres and Oceans, 21, 227–256.

Kostov, Y., Armour, K., & Marshall, J. (2013). Impact of the Atlantic Meridional Overturning Circulation on Ocean Heat Storage and Transient Climate Change. Geophysical Research Letters, 1–9. http://doi.org/10.1002/2013GL058998.1.

Lebedeff, S. A. (1988). Analytic solution of the box diffusion model for a global ocean. Journal of Geophysical Research, 93.

Lindzen, R. S., & Giannitsis, C. (1998). On the climatic implications of volcanic cooling. Journal of Geophysical Research, 103, 5929–5941. http://doi.org/10.1029/98JD00125

Marshall, J., Adcroft, A., Hill, C., Perelman, L., & Heisey, C. (1997). A finite-volume, incompressible Navier Stokes model for studies of the ocean on parallel computers. Journal of Geophysical Research, 102, 5753–5766.

Marshall, J., Hill, C., Perelman, L., & Adcroft, A. (1997). Hydrostatic, quasi-hydrostatic, and non hydrostatic ocean modelling. Journal of Geophysical Research, 102, 5733–5752.

Merlis, T. M., Held, I. M., Stenchikov, G. L., Zeng, F., & Horowitz, L. W. (2014). Constraining transient climate sensitivity using coupled climate model simulations of volcanic eruptions. Journal of Climate, 27(20), 7781–7795. http://doi.org/10.1175/JCLI-D-14-00214.1

Mignot, J., Khodri, M., Frankignoul, C., & Servonnat, J. (2011). Volcanic impact on the Atlantic Ocean over the last millennium. Climate of the Past Discussions, 7, 2511-2554.

Miller, G. H., Geirsdóttir, Á., Zhong, Y., Larsen, D. J., Otto-bliesner, B. L., Holland, M. M., … Björnsson, H. (2012). Abrupt onset of the Little Ice Age triggered by volcanism and sustained by sea-ice/ocean feedbacks. Geophysical Research Letters, 39, 1–5. http://doi.org/10.1029/2011GL050168

Neukom, R., Gergis, J., Karoly, D. J., Wanner, H., Curran, M., Elbert, J., … Mundo, I. (2014). Inter-hemispheric temperature variability over the past millennium. Nature Climate Change, 4. http://doi.org/10.1038/NCLIMATE2174

Otterå, O. H., Bentsen, M., Drange, H., & Suo, L. (2010). External forcing as a metronome for Atlantic multidecadal variability. Nature Geoscience, 3(10), 688.

Redi, M. (1982). Oceanic isopycnal mixing. Journal of Physical Oceanography, 12.

Robock, A. (2000). Volcanic eruptions and climate. Reviews of Geophysics, 38(2), 191–219. http://doi.org/10.1029/1998RG000054

Romanou, A., et al. "Role of the Ocean's AMOC in setting the Uptake Efficiency of Transient Tracers." Geophysical Research Letters.

Santer, B. D., Wigley, T. M. L., Doutriaux, C., Boyle, J. S., Hansen, J. E., Jones, P. D., ... & Taylor, K. E. (2001). Accounting for the effects of volcanoes and ENSO in comparisons of modeled and observed temperature trends. Journal of Geophysical Research: Atmospheres, 106(D22), 28033-28059

Sigl, M., Winstrup, M., McConnell, J. R., Welten, K. C., Plunkett, G., Ludlow, F., … Woodruff, T. E. (2015). Timing and climate forcing of volcanic eruptions for the past 2,500 years. Nature, 523(7562), 543–549. http://doi.org/10.1038/nature14565

Soden, B. J., Wetherald, R. T., Stenchikov, G. L., & Robock, A. (2000). Global Cooling After the Eruption of Mount Pinatubo : A Test of Climate Feedback by Water Vapor. Science, 296.

Stenchikov, G., Delworth, T. L., Ramaswamy, V., Stouffer, R. J., Wittenberg, A., & Zeng, F. (2009). Volcanic signals in oceans, 114, 1–13. http://doi.org/10.1029/2008JD011673

Stouffer, R. J. (2004). Time scales of climate response. Journal of Climate, 17(1), 209-217.

Wigley, T. M. L., Ammann, C. M., Santer, B. D., & Raper, S. C. (2005). Effect of climate sensitivity on the response to volcanic forcing. Journal of Geophysical Research: Atmospheres, 110(D9).

Winton, M., Takahashi, K., & Held, I. M. (2010). Importance of Ocean Heat Uptake Efficacy to Transient Climate Change. Journal of Climate, 23, 2333–2344. http://doi.org/10.1175/2009JCLI3139.1

Yokohata, T., Emori, S., Nozawa, T., Tsushima, Y., Ogura, T., & Kimoto, M. (2005). Climate response to volcanic forcing: Validation of climate sensitivity of a coupled atmosphere-ocean general circulation model. Geophysical Research Letters, 32(21).

Figure caption list

Fig. 1: Responses of the box model to an idealized Pinatubo eruption (-4 W/m^2 for a year) in the 1-box case (red) and 2-box cases (blue) in terms of the ratio of ocean mixing strength to the climatic feedback parameter $\mu = q/\lambda$ with $\lambda = 1.5 \mathrm{Wm}^{-2}\mathrm{K}^{-1}$. The 'area under the curve' is the same in all cases, but with a smaller peak and a longer 'tail' as q (or μ) increases.

Fig. 2: MITgcm responses to a Pinatubo-like forcing (-4 Wm^{-2} for a year) and a 10×Pinatubo forcing (-40 Wm^{-2} for a year) for the slab ocean in red and the full ocean configuration in blue. (a) Ensemble mean responses normalized with respect to their maximum cooling temperature. (b) Non-normalized responses for the Pinatubo forcing with the shaded envelopes of 5 ensemble

members for the slab ocean (red) and 10 ensemble members for the full ocean (blue). The solid lines are the corresponding ensemble mean. (c) Non-normalized responses for the 10×Pinatubo forcing with one ensemble member for the slab and full ocean respectively.

Fig. 3: MITgcm zonally averaged temperature anomaly in the ocean with depth and latitude in the full ocean configuration. The temperature evolution is shown for 2, 5 and 10 years after the eruption initiation in the left, middle and right panels respectively. The top panels are the mean responses of 10 ensemble members for the Pinatubo-like forcing (-4 Wm^{-2} for a year) and the bottom panels are the responses for a single ensemble member of the 10×Pinatubo forcing (-40 Wm^{-2} for a year). The thick black line represents the model-diagnosed mixed layer depth.

Fig. 4: MITgcm ensemble-mean response to a Pinatubo-like eruption (-4 Wm^{-2} for a year) every 10 years in the slab ocean (red) and full ocean (blue) configurations. The slab and full ocean configuration were run for 5 and 10 ensemble members respectively.

Fig. 5: 2-box model comprising a mixed layer of depth h_1 and a deeper ocean of depth h_2 with temperature anomalies T_1 and T_2 respectively. The model is driven from the top by an external forcing F and damped by the climate feedback λT_1. The two boxes exchange heat through the exchange parameter q.

Fig. 6: Temperature responses of the box model (solid lines) and the MITgcm (dotted lines) to an idealized Pinatubo forcing (-4 Wm^{-2} for a year). (a) 2-box model fit (solid blue) to the full ocean MITgcm response (dotted blue) with $r^2 = 0.87$ and 1-box model fit (solid red) to the slab ocean MITgcm response (dotted red) with $r^2 = 0.97$. The fit parameters are summarized in Table 1. (b) SST (dotted blue) and temperature at 120m depth (dotted yellow) from the MITgcm full ocean

configuration with the corresponding 2-box model temperatures T_1 (solid blue) and T_2 (solid yellow).

Fig. 7: 2-box model responses to an idealized Pinatubo forcing (-4 Wm^{-2} for a year) for a range of λ (or ECS) values. All other parameters are fixed to those in Table 1.

Fig. 8: Normalized temperature envelope T_{en} for a series of uniform and regularly spaced eruptions in the 2-box model. Each dot represents the peak cooling temperature after a new eruption. Parameter sensitivity is explored for (a) the climate sensitivity λ, (b) the ocean exchange parameter q, (c) the mixed layer depth h_1 and (d) the time interval between eruptions τ.

Fig. 9: (data from Sigl et al. 2015): (a) 2000-year reconstruction of global volcanic aerosol forcing from sulfate composite records from tropical (orange) and Northern Hemisphere (gray) eruptions. (b) 2000-year record of reconstructed summer temperature anomalies for Europe and the Arctic relative to 1961-1990 shown yearly (green) and as a 50-year running mean (orange). The 40 coldest single years are indicated with blue circles and the approximate duration of the Little Ice Age is shown.

Fig. 10: (a) Tropical volcanic forcing of the last millennium (A. LeGrande, NASA GISS, personal communication) divided into small ($>$ -4 $Wm^{-2}K^{-1}$) and large eruptions ($\leq$ -4 $Wm^{-2}K^{-1}$), (b*)* responses of the MITgcm full ocean (blue) and slab ocean (red) configurations to the volcanic forcing (c) 5-year running mean of (b) on a magnified scale; (d) Convolution response of the box model (solid line) and sensitivity to λ (shading). (e) 5-year running mean of the 2-box model response to the small (black) and large (gray) volcanic forcing.

Fig. A1. Linear albedo gradient imposed at the surface of the MITgcm model. The grid is in a cubed sphere configuration with 32×32 points per face, with a nominal horizontal resolution of

2.8°. The thick black lines indicate the solid ridges of the ‘double-drake’ setup extending from the North Pole to 35°S and set 90° apart.

Fig. A2: 1-D diffusion model with mixed layer depth h_1, deep ocean depth H, thermal diffusivity κ, climate feedback parameter λ, mixed layer temperature T_1 and deep ocean temperature T(z).

Fig. A3: Mixed layer temperature anomaly in the 1-D diffusion model (solid lines) and MITgcm (dotted lines) for a -40 $Wm^{-2}K$ pulse lasting 1 year. The red lines correspond to a slab ocean whereas the blue lines are for a full ocean. The response functions are shown for non-normalized values (left) and normalized by the corresponding peak cooling value (right).

Fig. A4: Time evolution of temperature profiles with depth for a 1-year forcing of -40 Wm^{-2} in (a) the 1-D diffusion model with $\kappa = 10^{-4}\ m^2s^{-1}$ and (b) the horizontally MITgcm full ocean configuration.

Parameter	Physical interpretation	Fit value
h_1	Mixed layer depth	43 m
h_2	Deeper ocean depth	150 m
λ	Climatic feedback	1.5 $Wm^{-2}K^{-1}$
q	Oceanic mixing	3.5 $Wm^{-2}K^{-1}$

Table 1: 2-box model parameters obtained by curve-fitting the SST response of the full ocean MITgcm to an idealized Pinatubo eruption (-4 W/m^2 for a year).

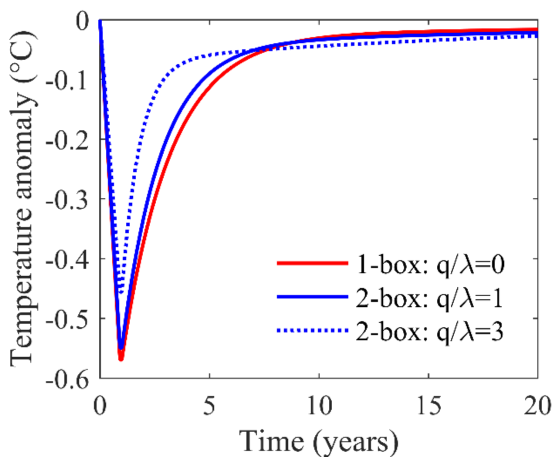

Fig. 1: Responses of the box model to an idealized Pinatubo eruption (-4 W/m^2 for a year) in the 1-box case (red) and 2-box cases (blue) in terms of the ratio of ocean mixing strength to the climatic feedback parameter $\mu = q/\lambda$ with $\lambda = 1.5 Wm^{-2}K^{-1}$. The ‘area under the curve’ is the same in all cases, but with a smaller peak and a longer ‘tail’ as q (or μ) increases.

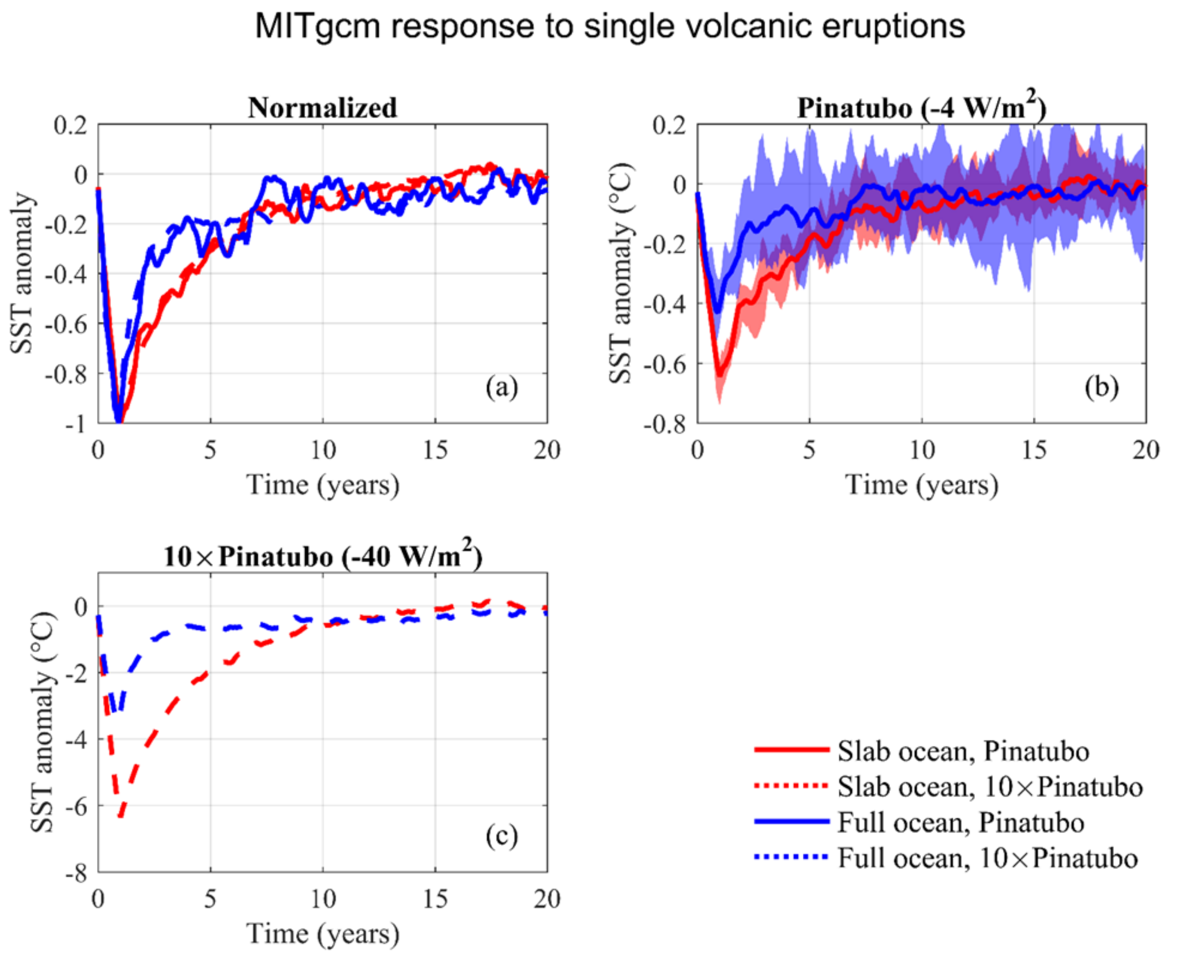

Fig. 2: MITgcm responses to a Pinatubo-like forcing (-4 Wm^{-2} for a year) and a 10×Pinatubo forcing (-40 Wm^{-2} for a year) for the slab ocean in red and the full ocean configuration in blue. (a) Ensemble mean responses normalized with respect to their maximum cooling temperature. (b) Non-normalized responses for the Pinatubo forcing with the shaded envelopes of 5 ensemble members for the slab ocean (red) and 10 ensemble members for the full ocean (blue). The solid lines are the corresponding ensemble mean. (c) Non-normalized responses for the 10×Pinatubo forcing with one ensemble member for the slab and full ocean respectively.

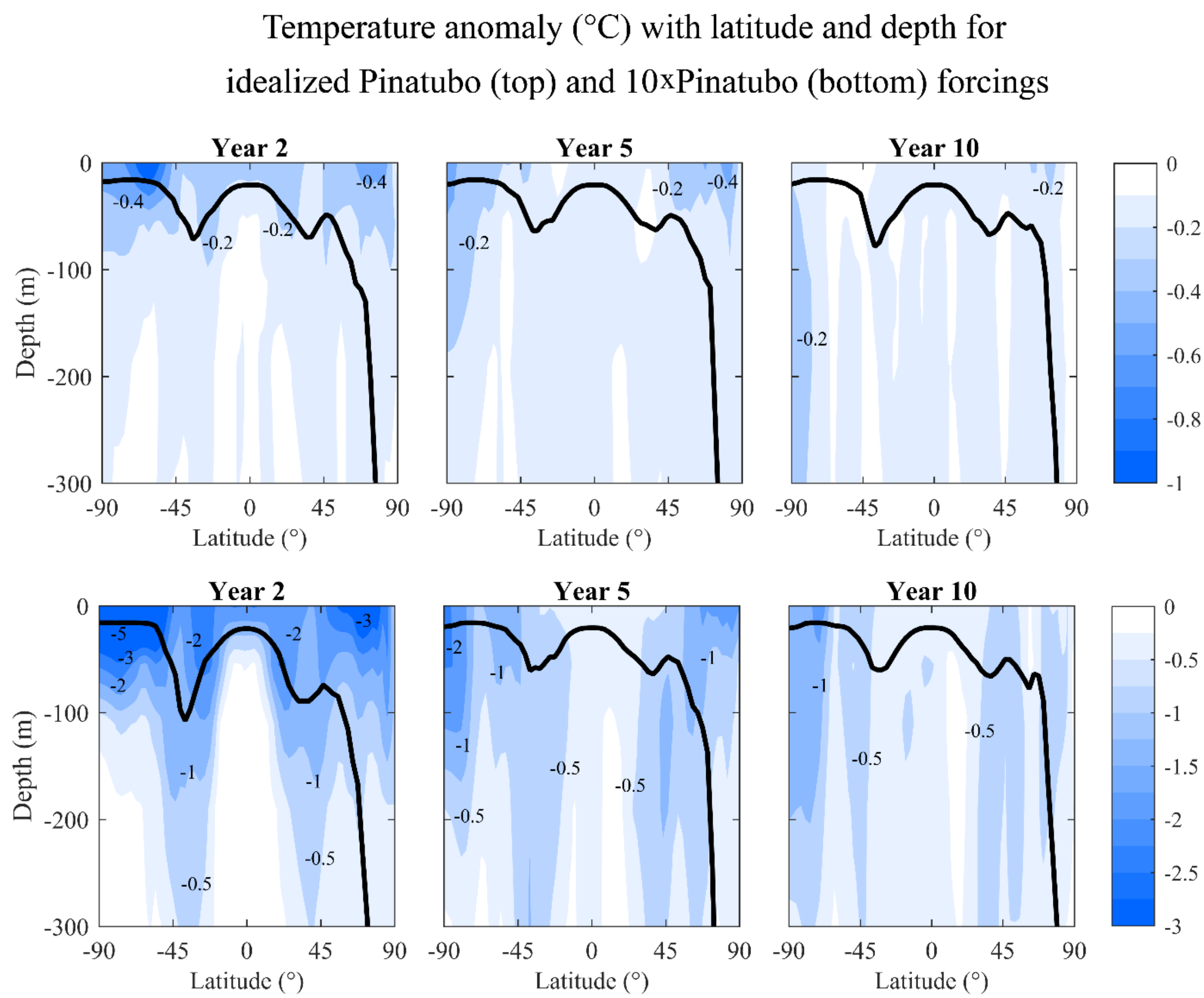

Fig. 3: MITgcm zonally averaged temperature anomaly in the ocean with depth and latitude in the full ocean configuration. The temperature evolution is shown for 2, 5 and 10 years after the eruption initiation in the left, middle and right panels respectively. The top panels are the mean responses of 10 ensemble members for the Pinatubo-like forcing (-4 Wm^{-2} for a year) and the bottom panels are the responses for a single ensemble member of the 10×Pinatubo forcing (-40 Wm^{-2} for a year). The thick black line represents the model-diagnosed mixed layer depth.

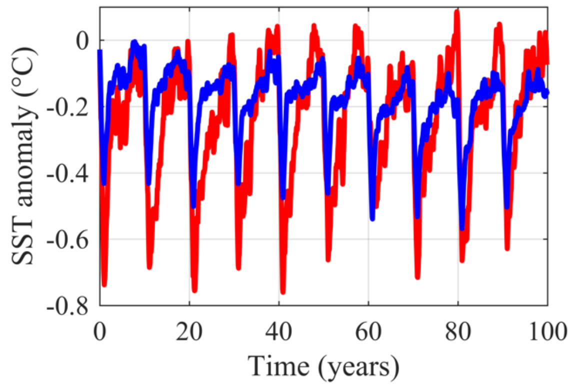

Fig. 4: MITgcm ensemble-mean response to a Pinatubo-like eruption (-4 Wm^{-2} for a year) every 10 years in the slab ocean (red) and full ocean (blue) configurations. The slab and full ocean configuration were run for 5 and 10 ensemble members respectively.

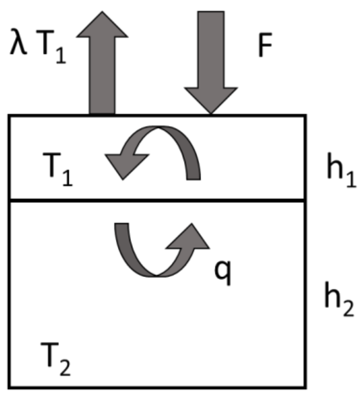

Fig. 5: 2-box model comprising a mixed layer of depth h_1 and a deeper ocean of depth h_2 with temperature anomalies T_1 and T_2 respectively. The model is driven from the top by an external forcing F and damped by the climate feedback λT_1. The two boxes exchange heat through the exchange parameter q.

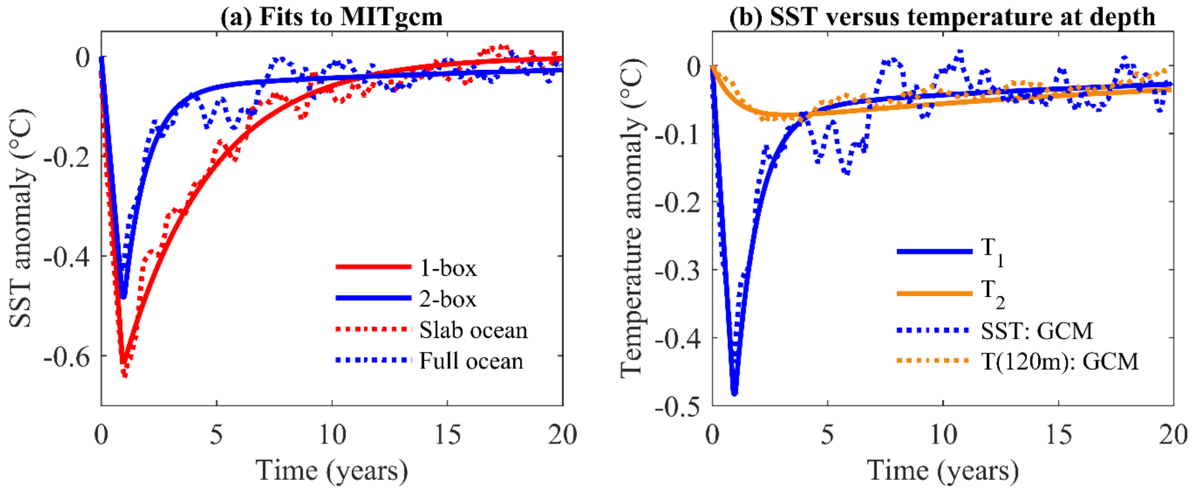

Fig. 6: Temperature responses of the box model (solid lines) and the MITgcm (dotted lines) to an idealized Pinatubo forcing (-4 Wm^{-2} for a year). (a) 2-box model fit (solid blue) to the full ocean MITgcm response (dotted blue) with $r^2 = 0.87$ and 1-box model fit (solid red) to the slab ocean MITgcm response (dotted red) with $r^2 = 0.97$. The fit parameters are summarized in Table 1. (b) SST (dotted blue) and temperature at 120m depth (dotted yellow) from the MITgcm full ocean configuration with the corresponding 2-box model temperatures T_1 (solid blue) and T_2 (solid yellow).

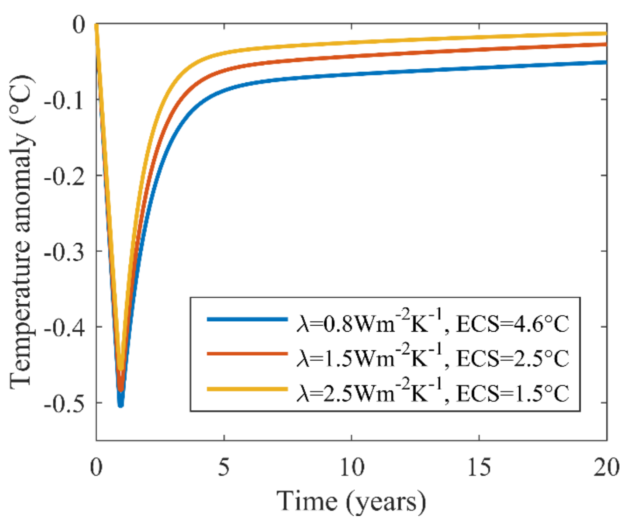

Fig. 7: 2-box model responses to an idealized Pinatubo forcing (-4 Wm^{-2} for a year) for a range of λ (or ECS) values. All other parameters are fixed to those in Table 1.

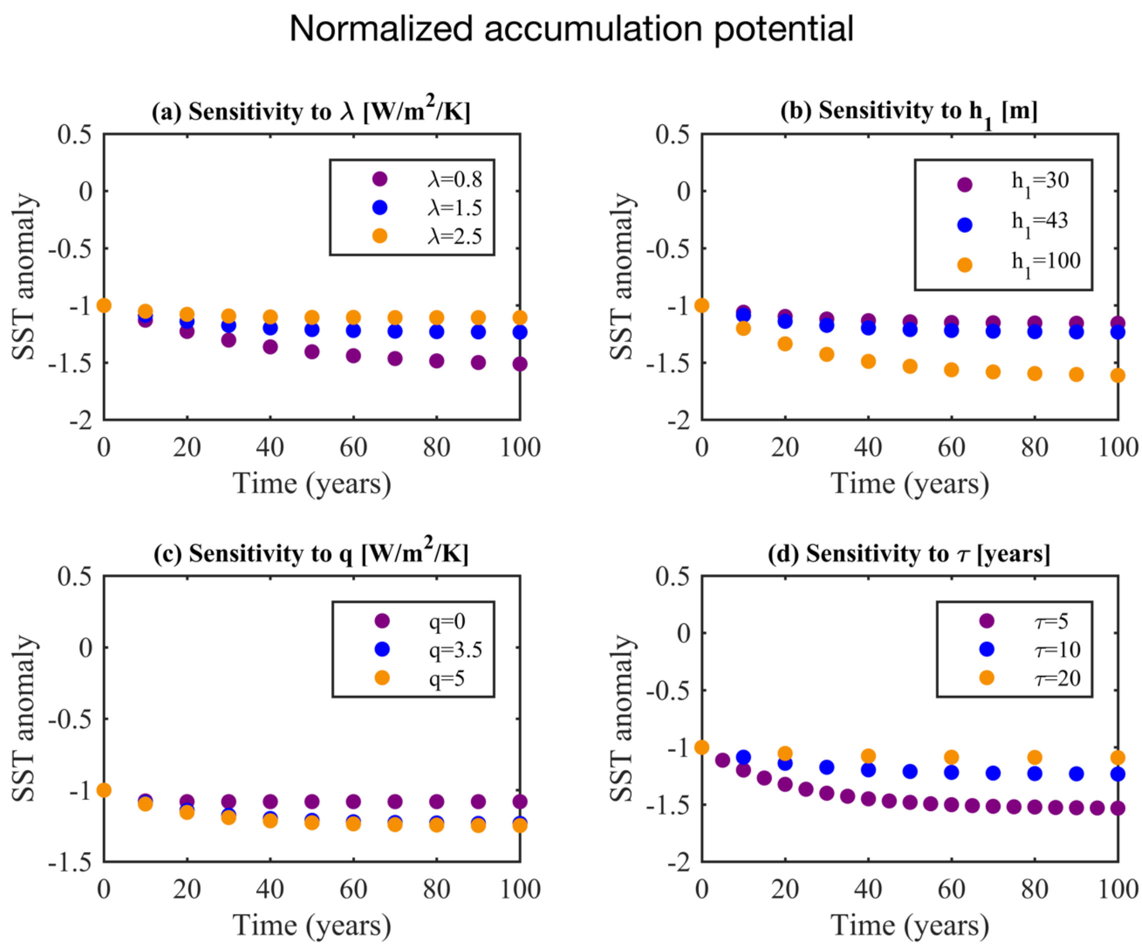

Fig. 8: Normalized temperature envelope T_{en} for a series of uniform and regularly spaced eruptions in the 2-box model. Each dot represents the peak cooling temperature after a new eruption. Parameter sensitivity is explored for (a) the climate sensitivity λ, (b) the ocean exchange parameter q, (c) the mixed layer depth h_1 and (d) the time interval between eruptions τ.

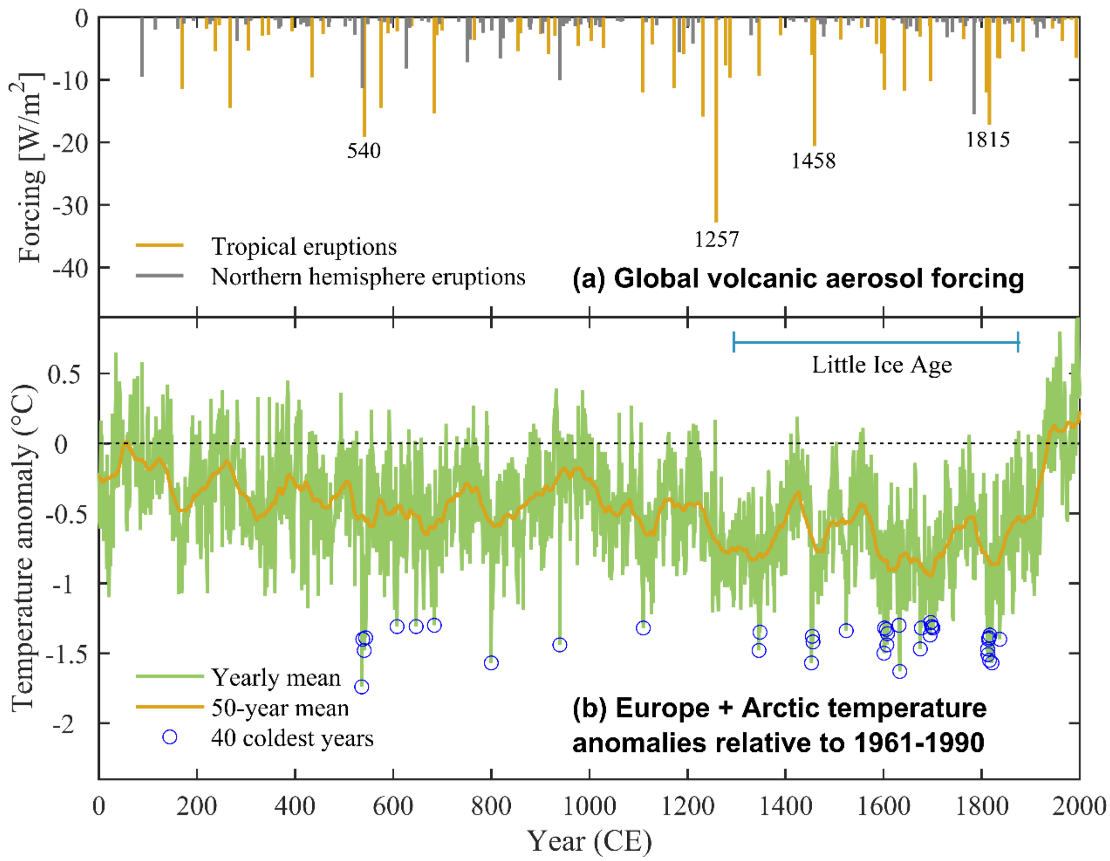

Fig. 9: (data from Sigl et al. 2015): (a) 2000-year reconstruction of global volcanic aerosol forcing from sulfate composite records from tropical (orange) and Northern Hemisphere (gray) eruptions. (b) 2000-year record of reconstructed summer temperature anomalies for Europe and the Arctic relative to 1961-1990 shown yearly (green) and as a 50-year running mean (orange). The 40 coldest single years are indicated with blue circles and the approximate duration of the Little Ice Age is shown.

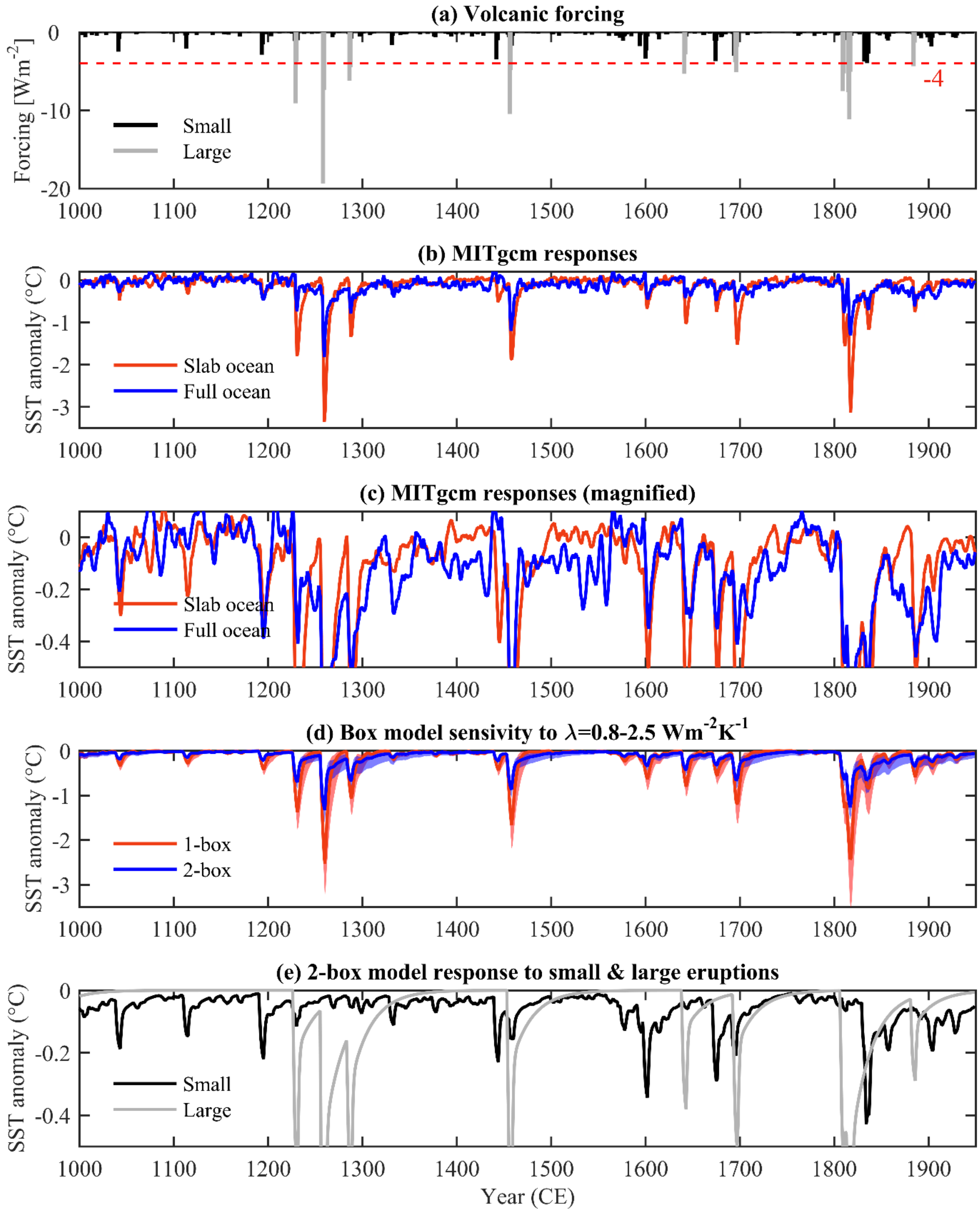

Fig. 10: (a) Tropical volcanic forcing of the last millennium (A. LeGrande, NASA GISS, personal communication) divided into small (> -4 $Wm^{-2}K^{-1}$) and large eruptions (≤ -4 $Wm^{-2}K^{-1}$),

(b) responses of the MITgcm full ocean (blue) and slab ocean (red) configurations to the volcanic forcing (c) 5-year running mean of (b) on a magnified scale; (d) Convolution response of the box model (solid line) and sensitivity to λ (shading). (e) 5-year running mean of the 2-box model response to the small (black) and large (gray) volcanic forcing.

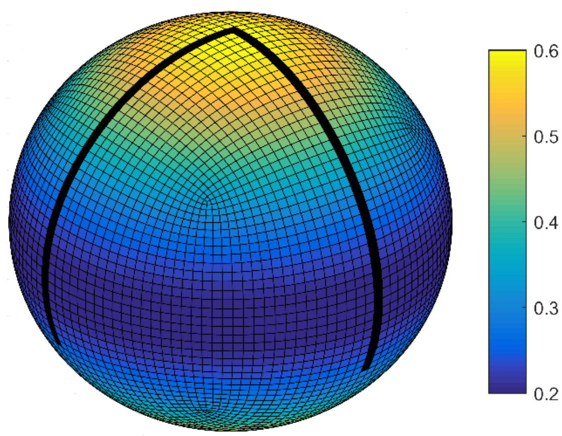

Fig. A1. Linear albedo gradient imposed at the surface of the MITgcm model. The grid is in a cubed sphere configuration with 32×32 points per face, with a nominal horizontal resolution of 2.8°. The thick black lines indicate the solid ridges of the 'double-drake' setup extending from the North Pole to 35°S and set 90° apart.

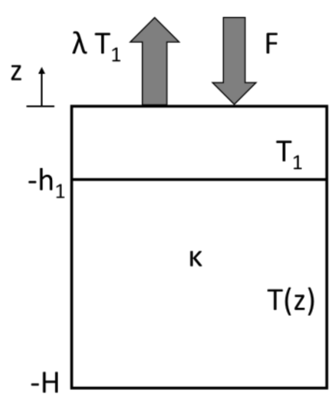

Fig. A2: 1-D diffusion model with mixed layer depth h_1, deep ocean depth H, thermal diffusivity κ, climate feedback parameter λ, mixed layer temperature T_1 and deep ocean temperature T(z).

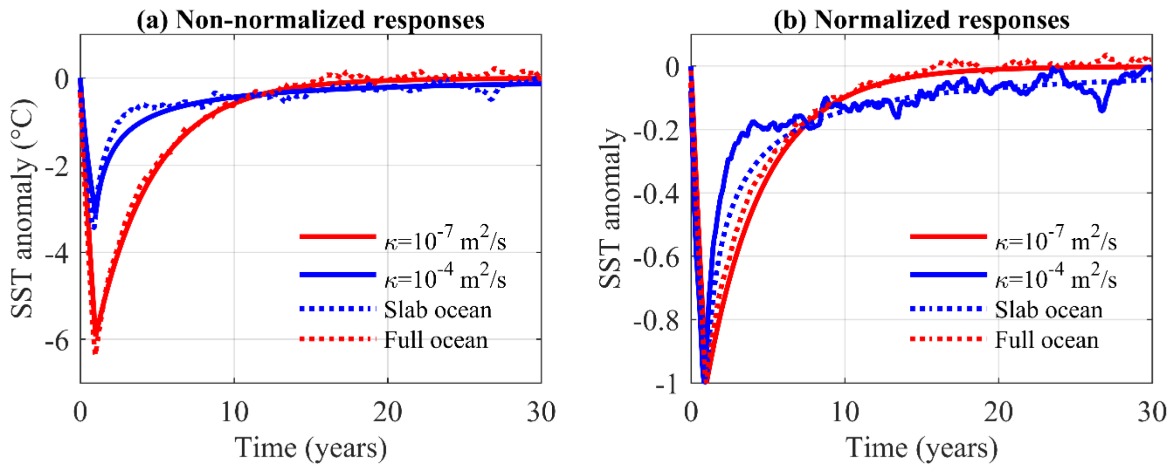

Fig. A3: Mixed layer temperature anomaly in the 1-D diffusion model (solid lines) and MITgcm (dotted lines) for a -40 Wm^{-2}K pulse lasting 1 year. The red lines correspond to a slab ocean whereas the blue lines are for a full ocean. The response functions are shown for non-normalized values (left) and normalized by the corresponding peak cooling value (right).

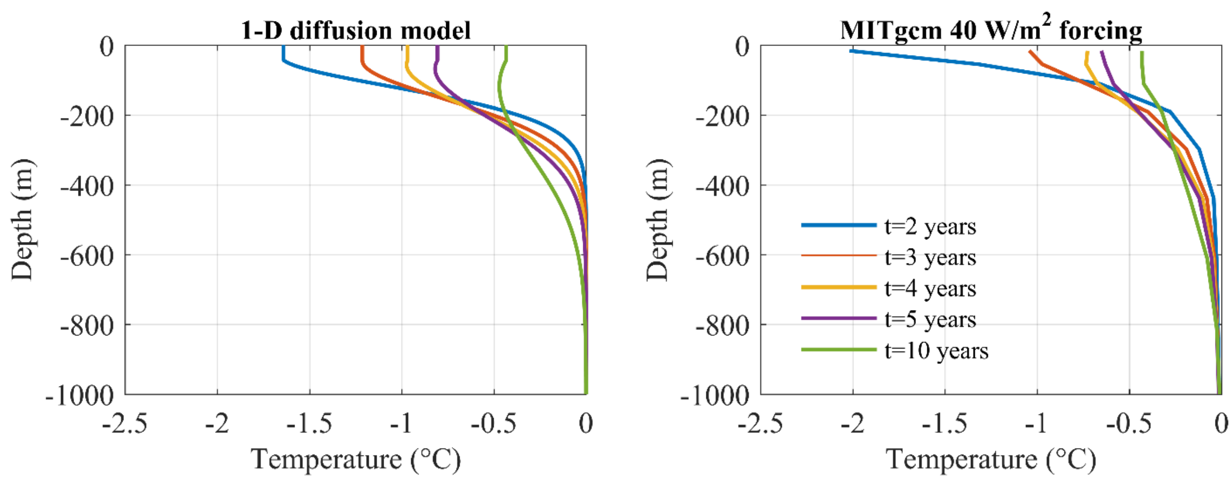

Fig. A4: Time evolution of temperature profiles with depth for a 1-year forcing of -40 Wm^{-2} in (a) the 1-D diffusion model with $\kappa = 10^{-4}$ m^{2}s^{-1} and (b) the horizontally MITgcm full ocean configuration.

Fig.1

Click here to access/download
Non-Rendered Figure
Fig1_lambda_q.png

Fig.2

Click here to access/download
Non-Rendered Figure
Fig2_MITgcm_single_erupt.png

Fig.3

Click here to access/download
Non-Rendered Figure
Fig3_lat_depth.png

Fig.4

Click here to access/download
Non-Rendered Figure
Fig4_MITgcm_10y.png

Fig.5

Fig.6

Click here to access/download
Non-Rendered Figure
Fig6_2box_fits.png

Fig.7

Click here to access/download
Non-Rendered Figure
Fig7_lambda_sens.png

Fig.8

Click here to access/download
Non-Rendered Figure
Fig8_accum_sens.png

Fig.9

Click here to access/download
Non-Rendered Figure
Fig9_sigl_data.png

Fig.10

Click here to access/download
Non-Rendered Figure
Fig10_historical.png

Fig.A1

Click here to access/download
Non-Rendered Figure
FigA1_3d_model.png

Fig.A2

Click here to access/download
Non-Rendered Figure
FigA2_1d_model.png

Fig.A3

Click here to access/download
Non-Rendered Figure
FigA3_1D_fit.png

Fig.A4

Click here to access/download
Non-Rendered Figure
FigA4_1D_profiles.png